JOURNAL OF SEMICONDUCTOR TECHNOLOGY AND SCIENCE, VOL.15, NO.2, APRIL, 2015
http://dx.doi.org/10.5573/JSTS.2015.15.2.232
ISSN(Print) 1598-1657
ISSN(Online) 2233-4866

Influence of the Recombination Parameters at the Si/SiO_2 Interface on the Ideality of the Dark Current of High Efficiency Silicon Solar Cells

Husain Kamal and Moustafa Ghannam

Abstract—**Analytical study of surface recombination at the Si/SiO_2 interface is carried out in order to set the optimum surface conditions that result in minimum dark base current and maximum open circuit voltage in silicon solar cells. Recombination centers are assumed to form a continuum rather than to be at a single energy level in the energy gap. It is shown that the presence of a hump in the dark I-V characteristics of high efficiency PERL cells is due to the dark current transition from a high surface recombination regime at low voltage to a low surface recombination regime at high voltage. Successful fitting of reported dark I-V characteristics of a typical PERL cell is obtained with several possible combinations of surface parameters including equal electron and hole capture cross sections.**

Index Terms—**Hump in dark current, non-ideality of dark current, silicon solar cells, surface recombination**

I. INTRODUCTION

High photovoltaic energy conversion is possible only if all types of carrier recombination in the solar cell are minimized. For that purpose, the substrate of state of the art high efficiency silicon solar cell is made of high quality Float Zone material with carrier lifetime exceeding a few ms. In such cells the bulk recombination is minimum and the cell performance is controlled by surface recombination.

The open circuit voltage of the PERL cell, which holds the 25% world record silicon cell efficiency is limited to 706 mV [1, 2] while an open circuit voltage reaching 750 mV and an efficiency as high as 25.6% have been recently reported in heterojunction silicon cells (HIT) [3, 4]. This recent improvement is due to smaller surface recombination in the HIT cell. It is projected that if surface recombination in the PERL cell could be reduced to bring the dark current density down to 10 fA/cm^2 its efficiency would rise to 26%.

The present work presents a clear understanding of the recombination process at the Si/SiO_2 interface and the influence of the surface recombination parameters on the dark current of the PERL cell. This is achieved through analytical modeling of surface recombination based on SRH recombination statistics [5] and on amphoteric recombination modeling [6-8]. The accuracy of the modelling is enhanced by assuming that recombination centers form a continuum distributed over all energy levels in the energy bandgap. Theoretical dark I-V characteristics are generated to reproduce measured dark I-V characteristics reported in the literature for a typical PERL cell.

II. DEPENDENCE OF THE EFFECTIVE SURFACE RECOMBINATION VELOCITY ON THE SURFACE PARAMETERS

As sketched in Fig. 1, a flux of electrons is injected

Manuscript received Dec. 22, 2014; accepted Feb. 14, 2015
Electrical Engineering Department, College of Engineering and Petroleum, Kuwait University, P.O. Box 5969, 13060 Safat, Kuwait
E-mail : husain.kamal@ku.edu.kw

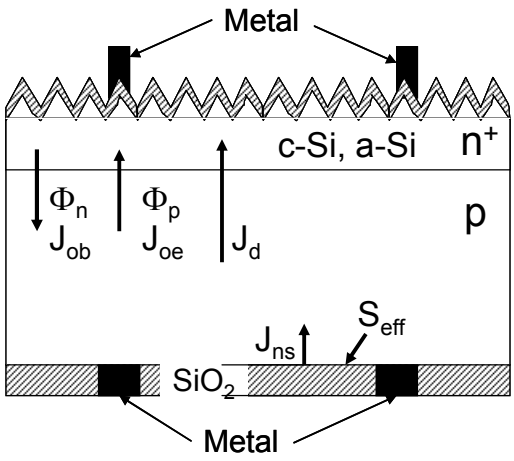

Fig. 1. Schematic cross section of an advanced n^+/p junction solar cell with SiO_2 back surface passivation (PERL cell).

across the forward biased junction and diffuses through the p-type base towards the back surface situated at $x = W$. Part of these electrons recombine in the bulk resulting in the bulk recombination current component J_{nb}. Excess electrons with a concentration $\Delta n(W)$ reach the edge of the back surface depletion region at the Si/SiO_2 interface and recombine with holes which results in the back surface recombination current component J_{ns}. Since back surface recombination sets the boundary condition at the back surface, both current components are affected by the value of S_{eff}. Consequently the value of S_{eff} is very critical in determining the dark current, the open circuit voltage and the cell efficiency.

The surface recombination models detailed in [7] are used in the present study. Both Shockley-Read-Hall (SRH) statistics and recombination through amphoteric recombination centers are considered. Using the same terminology as in [7] the SRH surface recombination rate U_s, repeated here for convenience, is given by:

$$U_s = \int_{E_v}^{E_c} \frac{v_{th} D_{it}(E_t)\left(p_s n_s - n_i^2\right) dE_t}{\left(\frac{n_s + n_i e^{(E_t - E_i)/kT}}{\sigma_p}\right) + \left(\frac{p_s + n_i e^{(E_i - E_t)/kT}}{\sigma_n}\right)} \qquad (1)$$

where $D_{it}(E_t)$ is the density of the energy- dependent recombination centers at the Si/SiO_2 interface, v_{th} is the electron thermal velocity, kT is the thermal energy, p_s, n_s and n_i are the hole, electron and intrinsic carrier concentrations at the surface, respectively, E_i and E_t are the intrinsic Fermi energy (mid-gap) and the recombination centre energy level, σ_n and σ_p represent the electron and hole capture cross sections of the centres. The effective surface recombination velocity is related to U_s through

$$S_{eff} = U_s / \Delta n(W) = \int_{E_v}^{E_c} \frac{v_{th} D_{it}(E_t) p_0 dE_t}{\left(\frac{n_s + n_i e^{(E_t - E_i)/kT}}{\sigma_p}\right) + \left(\frac{p_s + n_i e^{(E_i - E_t)/kT}}{\sigma_n}\right)} \qquad (2)$$

where p_o is the equilibrium hole concentration in the bulk which is equal to the p-type base surface doping concentration N_A.

Assuming negligible recombination in the very thin surface field (depletion) region, S_{eff} at the edge of the surface field region is obtained from

$$U_s = S_{eff} \Delta n(W) = q S_{eff} n_o \left(e^{V_F/V_T} - 1\right) \qquad (3)$$

where $\Delta n(W)$ has been replaced by $n_o(eV_F/V_T - 1)$ with n_o being the minority electron concentration in the p-type base, V_F is the carrier Quasi-Fermi energy separation at the back surface resulting from a forward bias V_j at the pn junction.

The effective surface recombination velocity S_{eff} is denoted as $S_{eff,SRH}$ for SRH model and as $S_{eff,amph}$ for amphoteric center model.

It is generally accepted that after annealing in forming gas or in hydrogen, the recombination centers at the Si/SiO_2 interface are uniformly distributed in the energy gap [9-11]. Hence $D_{it}(E_t)$ will be assumed to have a constant value D_{it}. In such a case the integral in (2) can be analytically performed resulting in [12]:

$$S_{eff} = 2 S_o p_o \frac{\ln\left[\frac{\frac{p_s}{K} + K n_s}{n_i}\right]}{\frac{p_s}{K} + K n_s} \qquad (4)$$

where

$$S_o = kT v_{th} D_{it} \sqrt{\sigma_n \sigma_p}$$

$$K = \sqrt{\sigma_n / \sigma_p}$$

The analytical expressions for S_{eff} in (4) help

significantly in understanding and predicting the behaviour of surface recombination under different operating conditions and the influence of the different parameters involved.

As described in [12] the surface carrier concentrations depend on the surface potential ψ_s (energy band bending) such that p_s and n_s in (4) are replaced by $p_o e^{-\psi s/V_T}$ and by $\Delta n(W) e^{\psi s/V_T}$, respectively Consequently

$$S_{eff} = 2S_o p_o \frac{\ln\left[\dfrac{\dfrac{p_o e^{-\psi_s/V_T}}{K} + K\Delta n(W) e^{\psi_s/V_T}}{n_i}\right]}{\dfrac{p_o e^{-\psi_s/V_T}}{K} + K\Delta n(W) e^{\psi_s/V_T}} \quad (5)$$

Note that the surface potential is positive when the p-type surface is depleted or inverted by the presence of a positive charge in the passivating SiO_2 layer. On the other hand, ψ_s is negative in surface accumulation.

The dependence of S_{eff} on the applied junction voltage V_j involves an iterative process since, for each junction voltage V_j, S_{eff} in (5) is calculated as a function of the resulting V_F at the surface. The latter is related to V_j through (3) which involves S_{eff} as will be detailed in section III. below.

1. S_{eff} versus Injection Range

We define "injection range", to be distinguished from injection level, a term that combines the injection level represented by $\Delta n(W)$, the surface potential ψ_s and the ratio between the capture cross sections in K. The value of S_{eff} is influenced by the injection range through the terms p_s/K and Kn_s in (4). The injection range switches from low when the $p_s/K >> Kn_s$ to high when $p_s/K << Kn_s$.

A. Low injection range

In the low injection range S_{eff} in (4) becomes

$$S_{eff} = 2S_o p_o \frac{\ln\left[\dfrac{p_o e^{-\psi_s/V_T}}{Kn_i}\right]}{(p_o e^{-\psi_s/V_T})/K} \quad (6a)$$

$$S_{eff} = 2S_o e^{\psi_s/V_T} K\left[\ln\left(\frac{1}{K}\right) + \left(\frac{\varphi_i - \psi_s}{V_T}\right)\right]$$

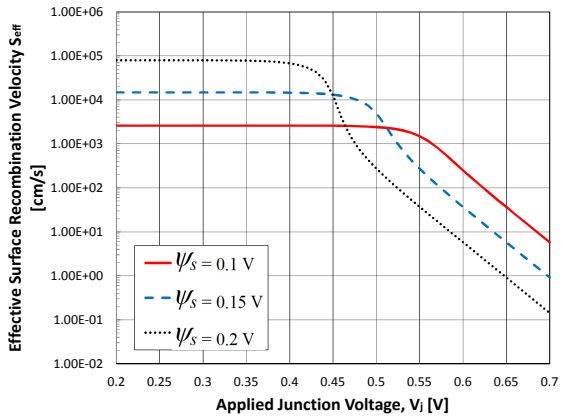

(a)

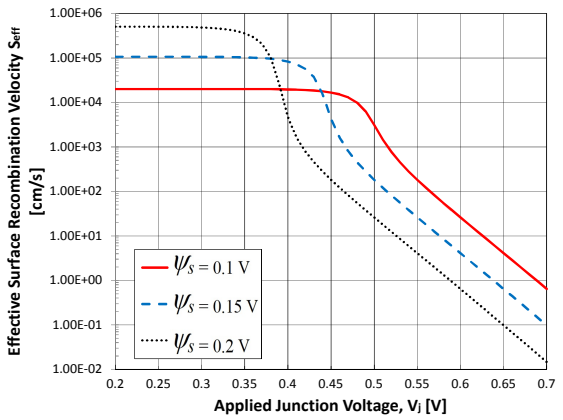

(b)

Fig. 2. (a) S_{eff} calculated according to SRH analytical model versus applied junction voltage for $D_{it} = 10^{10}$ /cm^2/eV, $\sigma_n = \sigma_p = 10^{-15}$ cm^2, and for ψ_s = 0.1 V, 0.15 V and 0.2 V, (b) S_{eff} calculated according to SRH analytical model versus applied junction voltage for $D_{it} = 10^{10}$ /cm^2/eV, $\sigma_n = 10^{-14}$ cm^2, $\sigma_p = 10^{-16}$ cm^2, and for ψ_s = 0.1, 0.15 and 0.2 V.

which is independent of $\Delta n(W)$ and of the applied junction voltage V_j as confirmed by the plateau regime in Fig. 2(a) displaying S_{eff} versus V_j. These results are generated for a typical device with a surface (base) doping concentration N_A = 1.5x10^{16} /cm^3, D_{it} = 10^{10} /cm^2/eV, $\sigma_n = \sigma_p$ = 10^{-15} cm^2 resulting in S_o = 2.586 cm/s which is a reasonable values for annealed Si/SiO$_2$ interface. Expression (6a) predicts an exponential increase in S_{eff} in the low injection range with increasing ψ_s which is confirmed in Fig. 2(a) showing a continuous increase in the value of S_{eff} in the plateau region as ψ_s increases from 0.1 V to 0.15 V to 0.2 V.

B. High injection range

With increasing junction voltage, the excess electron

concentration $\Delta n(W)$ increases and finally the operation enters the high injection range in which S_{eff} can be expressed as

$$S_{eff} = \frac{2S_o p_o e^{-\psi_s/V_T}}{K\Delta n(W)}\left[\ln\left(\frac{K\Delta n(W)}{p_o}\right)+\left(\frac{\varphi_i+\psi_s}{V_T}\right)\right] \quad (6b)$$

which predicts a continuous decline of S_{eff} with increasing $\Delta n(W)$ (i.e increasing V_j) as confirmed in Fig. 2(a). On the opposite to the plateau regime, the values of S_{eff} in the declining regime are smaller for higher ψ_s, as predicted by (6b).

2. Asymmetric Capture Cross Sections

When capture cross sections are asymmetric, the values of S_{eff} may change but its dependence on the injection range remains the same with a possible shift in the border voltage between the low and high range. For instance, keeping S_o unchanged with $\sigma_n = 10^{-14}$ cm^2 and $\sigma_p = 10^{-16}$ cm^2 (K = 10), the S_{eff}-V_j dependence shifts horizontally towards smaller values of V_j, as depicted in Fig. 2(b), and towards higher voltages when $K < 1$ ($\sigma_p > \sigma_n$).

3. Recombination via Amphoteric Recombination Centers

The interest in studying surface recombination through multi-charge Sah-Shockely recombination statistics [13] stems from the fact that the P_b centers created by dangling bonds at the Si/SiO$_2$ interface are amphoteric recombination centers [6]. The latter can be neutral with capture cross sections σ_n^0 and σ_p^0, positively charged and having a capture cross section σ_n^+ or negatively charged and having with a capture cross section σ_p^-. In addition, amphoteric centers are correlated with a positive energy. Details of the proposed surface recombination model through amphoteric centers can be found in [7]. This model is used here to calculate $S_{eff,amph}$ at the Si/SiO$_2$ interface and the results are compared with those obtained using the analytical SRH model. As depicted in Fig. 3(a), $S_{eff,amph}$ follows the same trend and is very close to $S_{eff,SRH}$ when all amphoteric capture cross sections (σ_n^0, σ_p^0, σ_n^+ and σ_p^-) and SRH capture cross sections (σ_n and σ_p) are equal.

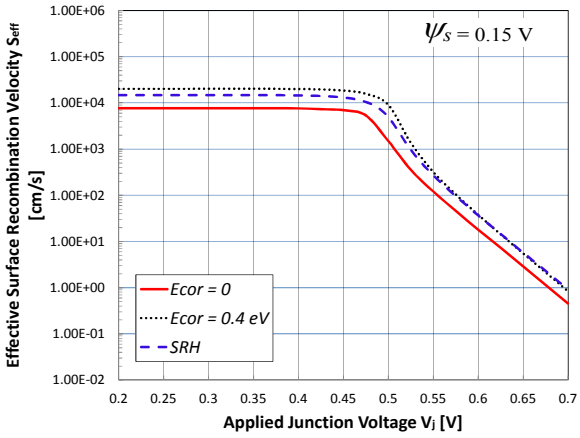

(a)

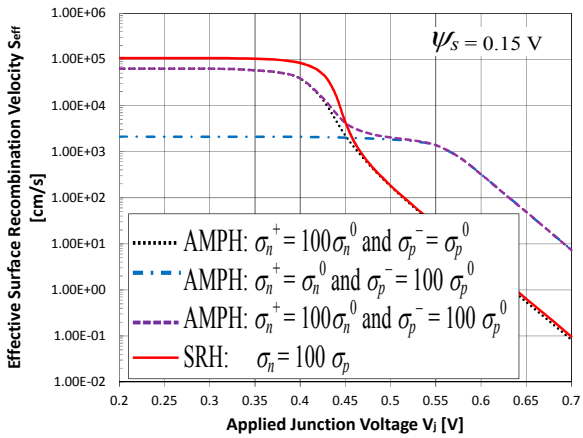

(b)

Fig. 3. (a) S_{eff} calculated according to SRH analytical model and to amphoteric recombination model versus applied junction voltage for $D_{it} = 10^{10}$ /cm^2/eV, $\sigma_n^0 = \sigma_n^+ = \sigma_p^0 = \sigma_p^- = \sigma_{p,SRH} = \sigma_{n,SRH} = 10^{-15}$ cm^2, for $\psi_s = 0.15$ V and for a correlation energy E_{cor} = 0 and 0.4 V, (b) S_{eff} calculated with SRH analytical model and with amphoteric recombination model versus applied junction voltage for $D_{it} = 10^{10}$ /cm^2/eV, for $\psi_s = 0.15$ V. 1. SRH: $\sigma_n = 100\sigma_p$, 2. AMPH: $\sigma_n^+ = 100\sigma_n^0$ and $\sigma_p^0 = \sigma_p^-$, 3. $\sigma_n^+ = \sigma_n^0$ and $\sigma_p^- = 100\sigma_p^0$, and 4. $\sigma_n^+ = 100\sigma_n^0$ and $\sigma_p^- = 100\sigma_p^0$.

It is found that the value of $S_{eff,amph}$ and the border voltage may vary significantly when $\sigma_n^+ \neq \sigma_n^0$ or $\sigma_p^- \neq \sigma_p^0$ but not its behaviour with junction voltage. On the other hand, a double asymmetry $\sigma_n^+ \neq \sigma_n^0$ and $\sigma_p^- \neq \sigma_p^0$, leads to a step in the S_{eff}-V_j dependence that clearly distinguishes recombination via amphoteric center [7]. The step becomes more pronounced when the asymmetry is large as depicted in Fig. 3(b) for $\sigma_n^+ = 100\sigma_n^0$ and $\sigma_p^- = 100\sigma_p^0$. Finally, $S_{eff,amph}$ is found to increase moderately with increasing correlation energy E_{cor}.

III. DARK I-V CHARACTERISTICS

1. Device Structure and Dark Current Expression

As described earlier, the solar cell under study sketched in Fig. 1 consists of a front thin n^+ emitter and a p-type back surface passivated with a SiO_2 layer. The total dark current density J_d is composed of holes injected into the emitter and electrons into the base (substrate) and is expressed as

$$J_d = J_o\left(e^{V_j/V_T} - 1\right) = \left(J_{ob} + J_{oe}\right)\left(e^{V_j/V_T} - 1\right) \qquad (7a)$$

where J_o is the total saturation current density, J_{ob} and J_{oe} represent the base and emitter components, respectively. One dimensional calculation of the dark current is carried out for the cell sections with SiO_2 passivated back surface. A constant value is assumed for the emitter saturation current density J_{oe}. The solution of the one-dimensional continuity equation and diffusion equation at low level injection results in an expression for J_{ob} given by

$$J_{ob} = \frac{qD_n n_o}{L_n}\frac{\frac{D_n}{L_n}\sinh\frac{W}{L_n} + S_{eff}\cosh\frac{W}{L_n}}{\frac{D_n}{L_n}\cosh\frac{W}{L_n} + S_{eff}\sinh\frac{W}{L_n}} \qquad (7b)$$

where D_n, L_n and n_o are respectively the electron diffusion coefficient, electron diffusion length and minority electron concentration in the p-type base, W is the base width and, S_{eff} is the effective surface recombination velocity at the back surface. Expression (7b) is obtained assuming low level injection and constant electron lifetime τ_n in the base, and using (3) as the back surface boundary condition. The excess electron concentration $\Delta n(x)$ is defined at any distance x in the base away from the junction and $\Delta n(W)$ is its value at the back surface.

The dependence of the dark current on applied junction voltage in (7a) is ideally exponential only if both J_{ob} and J_{oe} are independent of V_j. It is shown, in sections II that S_{eff} depends on $\Delta n(W)$ which depends on V_F and hence on V_j. Hence, according to (7b) a non-ideality is expected in the exponential I-V relationship unless: 1) S_{eff} is not sensitive to $\Delta n(W)$ like in the low injection plateau regime, 2) S_{eff} is too large such that it cancels out from (7b), and 3) S_{eff} is too small such that the terms involving S_{eff} in (7b) can be neglected. When S_{eff} is too large such that

$$S_{eff} >> \frac{D_n}{L_n}\coth\frac{W}{L_n} \qquad (8a)$$

J_{ob} in (7b) reaches its highest limit given by

$$J_{ob1} = q\frac{D_n}{L_n}n_o\coth\frac{W}{L_n} \qquad (8b)$$

which is independent of S_{eff} and leads to the plateau regime in the low injection range. On the other hand, if S_{eff} is too small such that

$$S_{eff} << \frac{D_n}{L_n}\tanh\frac{W}{L_n} \qquad (8c)$$

J_{ob} in (7b) reaches its lowest limit given by

$$J_{ob2} = q\frac{D_n}{L_n}n_o\tanh\frac{W}{L_n} \qquad (8d)$$

which is also independent of S_{eff} and will occur at the end of the tail of the declining regime in the high injection range.

2. Dark I-V Characteristics: Numerical Results

The relationship between the back surface recombination rate U_s and back surface recombination current density J_{ns} implies

$$\begin{aligned} J_{ns} &= J_{on,s}\left(e^{V_j/V_T} - 1\right) \\ &= qU_s = qS_{eff}n_o\left(e^{V_F/V_T} - 1\right) \end{aligned} \qquad (9a)$$

The latter is also expressed in terms of the device parameters through the solution of the electron continuity equation and electron diffusion current equation at $x = W$ resulting in

$$J_{on,s} = qn_o\frac{1}{\frac{1}{S_{eff}}\cosh\frac{W}{L_n} + \frac{L_n}{D_n}\sinh\frac{W}{L_n}} \qquad (9b)$$

As described in section II., iteration is necessary to calculate V_F and S_{eff} to determine J_{ob} in (9a). Fixing the surface potential ψ_s, for each value of V_j, the iteration starts by assigning an initial value to V_F (usually = V_j) resulting in an initial value for the excess electron surface concentration n_s and to a first guess for S_{eff} using (4). This first guess of S_{eff} is substituted in (9b) to get $J_{on,s.}$ The latter together with with V_j are substituted in the first equality in (9a) to get J_{ns}. This value of J_{ns} is now used in the second equality in (9a) while still using the first S_{eff} guess to determine a new value for V_F. The second round of the iteration starts and the procedure is reiterated until V_F and S_{eff} converge to final values. The base saturation current J_{ob} is then calculated by substituting the final S_{eff} value in (7b). The total diode current density J_d at the selected junction voltage V_j is calculated from (7a) assuming a value for J_{oe} as mentioned earlier. The complete dark I-V characteristics are obtained by repeating this procedure for different values of V_j within the range of interest.

The dark current is calculated for a typical PERL cell fabricated on Float-Zone p-type silicon wafer 280 μm thick having a base doping concentration N_A = 1.5x10^{16} /cm^3, an electron diffusion coefficient D_n = 26 cm^2/V.s and an electron diffusion length L_n = 0.137 cm. The emitter saturation current density J_{oe} is assumed to be equal to 10 fA/cm^2. The resulting dark I-V characteristics obtained with S_{eff} calculated using SRH surface recombination model with D_{it} = 10^{10}/cm^2/eV and equal capture cross sections σ_n = σ_p = 10^{-15} cm^2 are plotted in Fig. 4(a) for ψ_s = 0.1 V, 0.15 V, and 0.2 V. A set of curves generated with S_{eff} calculated using amphoteric recombination with D_{it} = 10^{10}/cm^2/eV, σ_n^+ = σ_n^0 = σ_p^- = σ_p^0 = 10^{-15} cm^2 is plotted in Fig. 4(b) also for surface potential ψ_s = 0.1 V, 0.15 V, and 0.2 V.

As discussed in section III. 1., the I-V characteristics displayed in Figs. 4(a) and (b) shows an ideal exponential sector with a high saturation current density at low voltage corresponding to high S_{eff} in the plateau regime. The saturation current may reach its high limit J_{ob1} in (8b) if condition (8a) is satisfied. On the other hand, the current shows another ideal exponential sector with smaller saturation current density at higher voltage corresponding to small values of S_{eff} in the tail end of the decline region where condition (8c) is satisfied and the saturation current reaches its low J_{ob2} limit in (8d). The

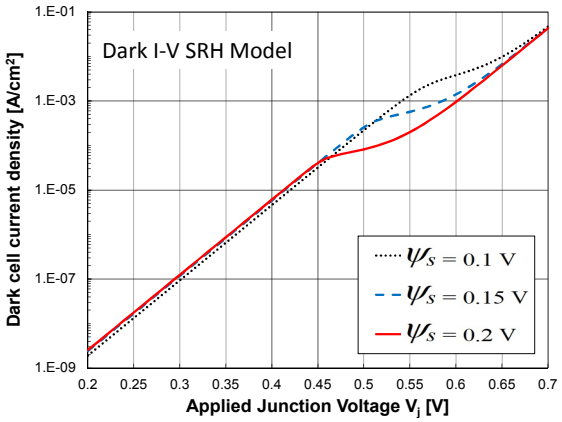

(a)

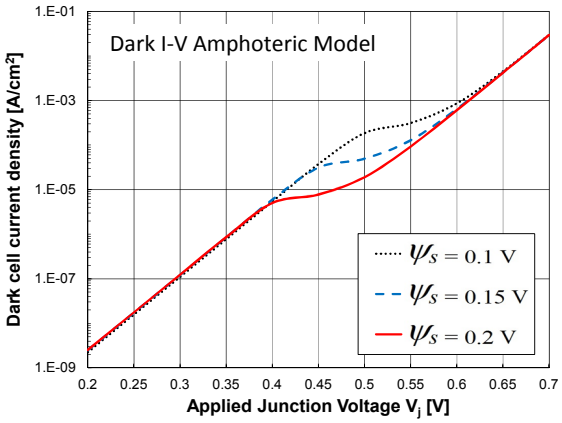

(b)

Fig. 4. (a) Calculated dark cell I-V characteristics for the PERL cell under consideration assuming J_{oe} = 10 fA/cm^2 and L_n = 0.137 cm for different values of ψ_s. S_{eff} is calculated according to SRH analytical model assuming D_{it} = 10^{10}/cm^2/eV, σ_n = σ_p = 10^{-15} cm^2, (b) Calculated dark cell I-V characteristics for the PERL cell under consideration assuming J_{oe} = 10 fA/cm^2 and L_n = 0.137 cm for different values of ψ_s. S_{eff} is calculated according to surface recombination model via amphoteric centers assuming D_{it} = 10^{10} /cm^2/eV, σ_n and σ_p for neutral and charged centers = 10^{-15} cm^2.

transition between the two ideal exponential sectors shapes a hump in the I-V characteristics.

The existence of the hump and its position in the I-V characteristics are influenced by the same parameters which affect S_{eff} namely: capture cross section ratio, surface potential and interface trap density. For instance, the hump shifts to a higher voltage at smaller values of ψ_s because the plateau regime extends to higher injection levels as depicted in Figs. 2(a) and (b). The hump may even disappear when ψ_s is very small since the plateau regime in this case extends outside the voltage range of interest, even if the capture cross sections are largely

asymmetric. Therefore, although asymmetry between capture cross sections is not ruled out, it is not accurate to systematically link the hump exclusively to large asymmetry $\sigma_n > \sigma_p$ by factors reaching 100 or even 1000 σ_p as previously suggested [14].

3. Fitting Experimental I-V Characteristics of a Typical PERL Cell

The experimental dark I-V characteristics for the PERL cell reported in [15] at T=25°C is reproduced by coupling the S_{eff} and J_{ob} models elaborated in the present work. The experimental dark saturation current density J_o deduced from the ideal exponential sectors of the measured I-V characteristics [15] amounts to 1050 fA/cm^2 at low voltage and to 62 fA/cm^2 at high voltage. This current includes: 1) J_{ob} bound by the back surface area passivated with SiO_2 (A_b), 2) the high limit J_{ob1} in (8b) at the metal contacted back surface areas (A_m), and 3) J_{oe}, the emitter current component across the total junction area (A_t), with $A_t = A_b + A_m$. Therefore, the total current is given by

$$J_{ob}A_b + J_{ob1}A_m + J_{oe}A_t = J_oA_t \qquad (10a)$$

Let's assume that at low bias condition (8a) is satisfied. In that case J_{ob} is equal to the high limit J_{ob1} such that

$$\begin{aligned} &J_{ob1}(A_b + A_m) + J_{oe}A_t = 1050A_t \quad \text{fA} \\ &J_{ob1} + J_{oe} = 1050 \quad \text{fA/cm}^2 \\ &\left(\frac{qD_n n_o}{L_n}\right)\coth\frac{W}{L_n} + J_{oe} = 1050 \quad \text{fA/cm}^2 \end{aligned} \qquad (10b)$$

On the other hand, since S_{eff} at the SiO_2 passivated areas at high bias is very small, J_{ob} will be given by J_{ob2} in (8d) leading to

$$\frac{qD_n n_o}{L_n}\left[r\tanh\frac{W}{L_n} + (1-r)\coth\frac{W}{L_n}\right] + J_{oe} = 62 \quad \text{fA/cm}^2 \qquad (10c)$$

where $r = A_b/A_t$ represents the fraction of the back surface passivated with SiO_2.

Setting J_{oe} to a minimum of 10 fA/cm^2 a set of reasonable values of the unknowns r, L_n, n_i satisfying (10b) and (10c) is extracted and includes r = 0.99, L_n = 1.37 mm and n_i = 1.02x10^{10} /cm^3, which is consistent with the most commonly used value reported in [16].

The high and low limits of S_{eff} are estimated from (8a) and (8c) to be 950 cm/s and 10 cm/s, respectively. Therefore any value of S_{eff} much larger than 950 cm/s would fit very well the I-V ideal exponential low voltage sector and any value for S_{eff} much smaller than 10 cm/s would fit very well the I-V ideal exponential high voltage sector. Fitting the hump region, however, requires an accurate knowledge of the value of S_{eff} and the shape of its decline. Therefore, the most accurate fitting of the I-V characteristics would be ensured if the calculated S_{eff}-V_j dependence matches that extracted from the current measurements. As depicted in Fig. 5, an excellent matching is achieved when S_{eff} is calculated according to SRH recombination assuming equal capture cross sections $\sigma_n = \sigma_p$ = 1.35x10^{-15} cm^2, D_{it} = 10^{10} /cm^2/eV, and a surface potential ψ_s = 0.175 V. The latter relates to a positive charge density Q_f in the oxide layer in the high 10^9 /cm^2 range which agrees well with values reported in several previous reports. An excellent matching is also possible when asymmetry in capture cross sections is traded with surface potential, for instance with ψ_s reduced from 0.175 V to 0.115 V and with σ_n = 1.35x10^{-14} cm^2 and σ_p = 1.35x10^{-16} cm^2. Excellent matching can also be achieved with several combinations of the parameters.

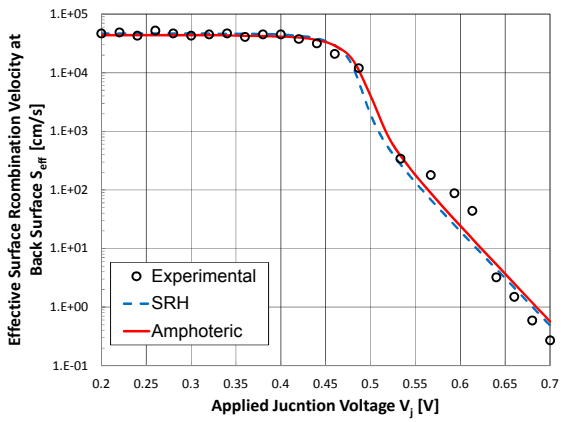

Fig. 5. Matching S_{eff} calculated according to SRH model and amphoteric recombination model with data extracted from measured PERL cell dark I-V characteristics [15]. 1. SRH: $\sigma_n = \sigma_p$ = 1.35x10^{-15}, ψ_s = 0.175 V, 2. AMPH: σ_n^0 = 3.2x10^{-16} cm^2, $\sigma_n^+ = 10\sigma_n^0$, σ_p^0 = 1.6x10^{-15} cm^2, $\sigma_p^- = \sigma_p^0$, E_{cor} = 0.3 eV and ψ_s = 0.165 V. For both models D_{it} = 10^{10} /cm^2/eV.

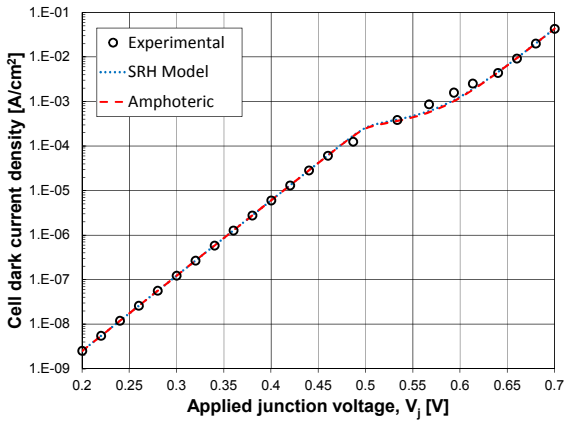

Fig. 6. Fitting measured PERL cell dark I-V characteristics [15] with S_{eff} calculated according to SRH and amphoteric recombination models with the same surface parameters leading to the S_{eff} matching displayed in Fig. 5.

The experimental S_{eff}-V_j dependence is equally well matched when S_{eff} is calculated according to the amphoteric center recombination model, as depicted in Fig. 5 for instance assuming a surface potential ψ_s = 0.165 V, D_{it} = 10^{10} /cm^2/eV, σ_n^0 = 3.2x10^{-16} cm^2, σ_p^0 = 1.6x10^{-15} cm^2, $\sigma_n^+ = 10\sigma_n^0$ and $\sigma_p^- = \sigma_n^0$. Other combinations of parameters would also lead to similar results.

Having succeeded the matching of calculated/ measured S_{eff}, a successful and accurate fitting of the measured dark I-V characteristics is systematically ensured as displayed in Fig. 6 for both SRH and amphoteric center recombination models.

IV. Impact of the Hump on Solar Cell Performance under Illumination

The impact of the hump on the performance of the cell under study is clear in Fig. 7 displaying the illuminated I-V characteristics in the voltage range close to the maximum power point. These characteristics are obtained by superposing a photogenerated current J_{sc} = 40 mA/cm^2 to the dark I-V characteristics. The influence of the hump is seriously detrimental at values of surface potential smaller than 0.15 V which is an indication that the hump in the dark I-V characteristics occurs at a voltage close to that of the maximum power point.

The open circuit voltage V_{oc} of the cell under study is calculated from the relationship

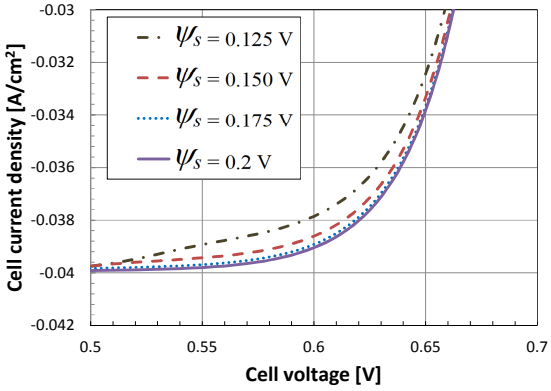

Fig. 7. I-V curves under illumination in the voltage range close to the maximum power point with emphasis on discrepancies due to hump in the dark I-V characteristics.

$$V_{oc} = \frac{kT}{q}\ln\left(\frac{J_{sc}}{J_o}\right) \tag{11}$$

and plotted versus surface potential ψ_s in Fig. 8(a). V_{oc} has a constant maximum value of 698 mV at high values of surface potential when the hump occurs in the lower voltage range and the dark saturation current density is at its minimum value of 62 fA/cm^2. The minimum value of V_{oc} occurs at ψ_s = 0.03 V and is equal to 673 mV which corresponds to J_{ob} = 167 fA/cm^2 and hence to a higher S_{eff}. The fact that V_{oc} and J_{ob} are affected by the value of S_{eff} means that the latter lies in the intermediate range between the high and the low limits defined in (8a) and (8c). Hence, to avoid performance degradation, the back interface passivation should be designed such that ψ_s is outside this critical range. With a large positive oxide charge density, typically in the high 10^9 /cm^2 range, the electron surface concentration is high enough to shift S_{eff} to the tail end of the declining regime with very small values bringing J_{ob} to its low limit (8d). Alternatively, with a large negative charge in the oxide ψ_s is negative leading to surface accumulation with holes. In such a case the value of S_{eff} in the plateau regime is very small which shifts the hump to the very high voltage range outside the range of interest. Such a p-type back surface passivation scheme has been successfully realized in recent years using a few atomic layer thick Al_2O_3 layer containing a large density of negative charge and deposited by atomic layer deposition (ALD) [17].

As depicted in Fig. 8(b), the hump affects the Fill Factor (FF) seriously if it occurs close to the maximum

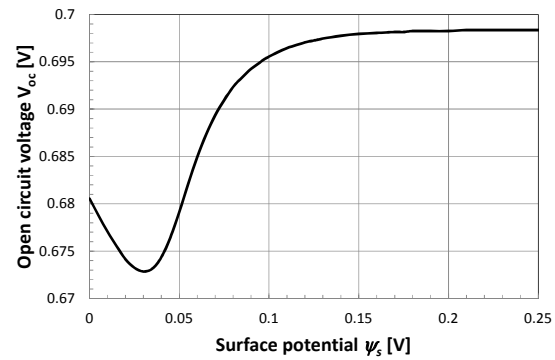

(a)

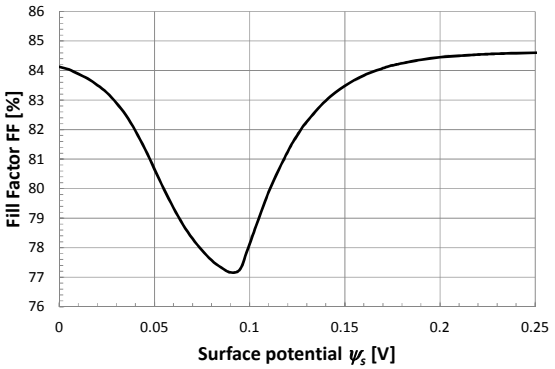

(b)

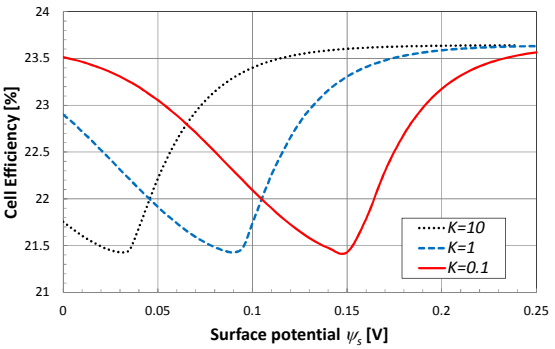

(c)

Fig. 8. (a) Open circuit voltage of the PERL cell under study, with surface parameters described in section III. 1. and equal capture cross sections (K=1), as a function of the surface potential, (b) Fill Factor of the PERL cell under study with surface parameters described in section III. 1. and equal capture cross sections (K=1) as a function of the surface potential, (c) Conversion efficiency of the PERL cell with surface parameters given in section III. 1., as a function of the surface potential for three different capture cross section ratios: K = 0.1, 1, and 10.

power point. For instance, the FF calculated from the I-V characteristics under illumination decreases from a maximum of 84.6% when ψ_s is larger than 0.2 V to a minimum of 77.1% when ψ_s = 0.08 V as depicted in Fig. 8(b).

Such degradations in V_{oc} from 698 mV to 673 mV and in FF from 84.6% to 77.1% lead to a significant drop of the efficiency of the cell from 23.64 % to 21.42% within the critical surface potential range, as depicted in Fig. 8(c). The same conclusion can also be drawn if the capture cross sections are not equal ($K \neq 1$) but with a shift in the critical surface potential range as depicted in Fig. 8(c).

V. Summary And Conclusions

Modelling of surface recombination following Shockley-Read-Hall and amphoteric recombination statistics confirm that the switch of S_{eff} from high values at low voltage to smaller values at high voltage is responsible for shaping a hump in the dark I-V characteristics of the cell. The transition voltage from low to high voltage range is determined by the values of the surface potential, values and ratio of electron to hole capture cross sections. Excellent fitting of measured dark I-V characteristics is obtained with SRH as well as with amphoteric recombination statistics with different combinations of surface potential, recombination center density, capture cross sections values and ratios. Hence, it is not possible from the dark I-V characteristics to extract a value for any of the surface parameters independently of other parameters without other supporting independent confirmation. Excellent fitting with equal capture cross sections is also obtained which indicates that the presence of a hump in the I-V characteristics does not necessarily mean that capture cross sections are largely asymmetric as previously suggested [14]. The degradation of the cell performance can be avoided if the hump is properly positioned in the I-V characteristics well below the maximum power point. This can be done by controlling the surface potential through varying the fixed charge density in the SiO_2.

As mentioned earlier, the best reported efficiency for a PERL cell amounts to 25% with a short circuit current density of 42 mA/cm^2 and an open circuit voltage of 706 mV. The corresponding dark saturation current density estimated to 46 fA/cm^2. Given the high quality of the Float Zone silicon bulk material with a diffusion length of a few times longer than the base width, the dark current is practically completely due to surface recombination. Maintaining the photocurrent at 42

mA/cm^2, the efficiency may attain 26% if the open circuit voltage could reach 734 mV which corresponds to a maximum surface recombination saturation current density of 15.6 fA/cm^2. The present work indicates that even with very small values of S_{eff} it is hard to reach such a small current in the PERL cell. On the other hand, a V_{oc} exceeding 740 meV has been reached in the HIT cell implementing an amorphous silicon-crystalline silicon (a-Si:H/c-Si) interface [3]. Therefore, if the PERL cell technology with its very high short circuit current could be combined with a HIT-like back surface passivation the limit of 26% could be possibly exceeded. A step towards this goal has been reached with the announcement of an efficiency of 25.6% with a back sided HIT cell [4].

ACKNOWLEDGMENTS

This work is supported by Kuwait University Research Administration Grant [EE03/12].

REFERENCES

[1] M. Green, K. Emery, Y. Hishikawa, W. Warta, and E. Dunlop, "Solar cell efficiency tables (version 39)", Progress in Photovoltaics: Research and Application, Vol.20, No.11, pp.12-20, 2012.

[2] J. Zhao, A. Wang, and M. A. Green, "High efficiency PERL and PERT silicon solar cells on FZ and MCZ substrates", Solar Energy Materials and Solar Cells, Vol.65, No.(1-4), pp.429-435, 2001.

[3] M. Taguchi, A. Yano, S. Tohoda, K. Matsuyama, Y. Nakamura, T. Nishiwaki, and E. Maruyama, "24.7% record efficiency HIT solar cell on thin silicon wafer", IEEE Journal Of Photovoltaics, Vol.4, No.1, pp.96-99, 2014.

[4] K. Masuko, M. Shigematsu, T. Hashiguchi, D. Fujishima, M. Kai, N. Yoshimura, T. Yamaguchi, Y. Ichihashi, T. Mishima, N. Matsubara, T. Yamanishi, T. Takahama, M. Taguchi, E. Maruyama, S. Okamoto, "Achievement of more than 25% conversion efficiency with crystalline silicon heterojunction solar cell", IEEE Journal of Photovoltaics, Vol.4, No.6, pp.1433-1435, 2014.

[5] W. Shockley, and W. T. Read, "Statistics of the recombination of holes and electrons", Physical Review, Vol.87, No.5, pp.835-842, 1952.

[6] S. Steingrube, R. Brendel, and P. Altermatt, "Limits to model amphoteric defect recombination via SRH statistics", Physica Status Solidi A, Vol.209, pp.390-400, 2012.

[7] M. Y. Ghannam, and H. A. Kamal, "Modeling surface recombination at the p-type Si/SiO_2 interface via dangling bond amphoteric centers", Advances in Condensed Matter Physics, Hindawi Publishing Corporation, Vol.2014, Article ID.857907, 9 pages. 2014.

[8] S. Olibet, E. Vallat-Sauvain, L. Fesquet, C. Monachon, A. Hessler-Wyser, J. Damon-Lacoste, S. De Wolf, and C. Ballif, "Properties of interfaces in amorphous/crystalline silicon heterojunctions," Physica Status Solidi A, Vol.207, pp. 651-656, 2010.

[9] W. Fussel, M. Schmidt, H. Angermann, G. Mende, and H. Flietner, "Defects at the Si/SiO_2 interface: their nature and behaviour in technological process and stress", Nuclear Instruments and Methods in Physics Research A, Vol.377, pp. 177-183, 1996.

[10] P. J. Caplan, E. H. Poindexter, B. E. Deal and R. R. Razouk, "ESR centers, interface states, and oxide fixed charge in thermally oxidized silicon wafers," Journal of Applied Physics, Vol.50, pp.5847-5854, 1979.

[11] R. R. Razouk and B. E. Deal, "Dependence of interface state density on silicon thermal oxidation process variables", Journal of the Electrochemical Society, Vol.126, pp.1573-1581, 1979.

[12] M. Y. Ghannam, R. P. Mertens, R. De Keersmaecker, and R. J. van Overstraeten, "Electrical characterization of the boron-doped Si-SiO_2 interface", IEEE Transactions on Electron Devices, Vol.32, pp.1264-1271, 1985.

[13] C. T. Sah and W. Shockley, "Electron-hole recombination statistics in semiconductors through flaws with many charge conditions", Physical Review, Vol.109, No.4, pp.1103-1115, 1958.

[14] S. Glunz, D. Biro, S. Rein, and W. Warta, "Field-effect passivation of the SiO_2-Si interface", Journal of Applied Physics, Vol.86, No.1, pp.683-691, 1999.

[15] J. Zhao, A. Wang, X. Dai, M.A. Green and S. Wenham, "Improvements in silicon solar cell performance", Proceedings of the 22nd IEEE

Photovoltaic Specialists Conference, pp.399-402, Las Vegas, NV, USA, 1991.

[16] A. B. Sproul, M.A. Green, and J. Zhao, "An Improved value for the silicon intrinsic carrier concentration at 300 K", Applied Physics letters, Vol.57, pp.255-257, 1990.

[17] J. Schmidt, A. Merkle, R. Brendel, B. Hoex, M.C.M Van de Sanden, W.M.M. Kessels, "Surface passivation of high efficiency silicon solar cells by atomic-layer –deposited Al_2O_3," Progress in Photovoltaics; Research and Applications, vol. 16, no. 6, pp. 461-466, 2008.

Husain A. Kamal is an assistant professor with the Department of Electrical Engineering at the Kuwait University. He received his BS degrees in Biomedical engineering from Marquette University (Milwaukee, Wisconsin) in 1989, and his MS and PhD. degree in electrical engineering (with specialization in Microelectronics) from University of Wisconsin (Madison, Wisconsin) in 1995 and 1997, respectively. Dr. Kamal's research interests are Bioinstrumentation, Microelectronic circuits/devices, Semiconductor devices, Optical computing, Optical pattern recognition.

M.Y Ghannam received the Ph.D degree in Electrical Engineering from the Catholic University of Leuven, Belgium in 1985. From 1985-1987 he was a postdoctoral fellow at the EE department, Stanford University, California, and from 1987 to 1993 he held positions at Cairo University, Egypt and the Interuniversity Microelectronics Center IMEC, Leuven, Belgium. In 1993 he joined Kuwait University as an Associate Professor, then Full Professor. During 2004-2006 he was a Professor at the College of Sciences and Engineering at the American University in Cairo (AUC). He re-joined EE Department at Kuwait University in 2006. M. Y. Ghannam is author and coauthor of 50 refereed journal papers, a hundred international conference papers, and five book chapters, all related to microelectronic devices and technology, and to silicon solar cells. He holds one US and one European/Japaneese patent and received several research awards. He served in committees of several IEEE conferences, and as an associatee editor of the Kuwait Journal of Sciences and Engineering. M.Y. Ghannam is a Senior member of the IEEE Electron Device Society.